

APPLICATION OF THE LS-STAG IMMERSSED BOUNDARY METHOD FOR NUMERICAL SIMULATION IN COUPLED AEROELASTIC PROBLEMS

VALERIA V. PUZIKOVA AND ILIA K. MARCHEVSKY

Bauman Moscow State Technical University (BMSTU)
Applied Mathematics department
Russia, 105005 Moscow, 2nd Baumanskaya, 5
e-mail: valeria.puzikova@gmail.com, iliamarchevsky@mail.ru

Key words: Immersed Boundary Methods, The LS-STAG Method, Coupled Aeroelastic Problems, The Spalart-Allmaras RANS Model, Multigrid Methods

Abstract. A software package is developed for numerical solution of the Navier-Stokes and Reynolds-averaged Navier-Stokes equations by using the LS-STAG method. The flow past an in-line oscillating circular airfoil was computed to verify the numerical method and the developed software package. Some numerical results are also presented for simulation of a circular airfoil wind resonance phenomenon and wind turbine rotors autorotation.

1 INTRODUCTION

Coupled aeroelastic problems appear when simulating autorotation and auto-oscillations phenomena, in particular, airfoil wind resonance. Such problems are complicated for numerical solution, since it is necessary to take into account interference between the flow and moving immersed body. In case of sufficiently massive body, coupled aeroelastic problems can be solved using step-by-step numerical algorithm, firstly simulating flow around a body moving with known parameters and then computing the dynamics of the body with known hydrodynamic loads.

Immersed boundary methods [1] are useful for numerical simulation in coupled aeroelastic problems, since they do not require a coincidence of cell edges and boundaries of the computational domain, and allow to solve problems when domain shape is irregular or it changes in the simulation process due to aeroelastic body motion. The main advantage of these methods is that we don't need mesh reconstruction at each time step.

In the present study, the LS-STAG cut-cell immersed boundary method [2] is used. This method allows to solve problems on the Cartesian grid. Immersed boundary is represented with the level-set function [3]. Linear systems resulting from the LS-STAG discretization of the Navier-Stokes or Reynolds-averaged Navier-Stokes equations, are solved using the

BiCGStab method [4] with the ILU- and multigrid [5, 6] preconditioning. An original algorithm for the solver cost-coefficient estimation [7] is used for the optimal parameters of the multigrid preconditioner choice.

2 GOVERNING EQUATIONS

The problem is considered in 2D unsteady case when the flow around an airfoil assumed to be viscous and incompressible. The continuity and momentum equations are the following:

$$\nabla \cdot \mathbf{v} = 0, \quad \frac{\partial \mathbf{v}}{\partial t} + (\mathbf{v} \cdot \nabla) \mathbf{v} = \frac{1}{\rho} \nabla p + \nu \Delta \mathbf{v}. \quad (1)$$

The boundary conditions on the computational domain are the following:

$$\mathbf{v}|_{\text{inlet}} = \mathbf{v}_\infty, \quad \frac{\partial \mathbf{v}}{\partial \mathbf{n}}|_{\text{outlet}} = 0, \quad \frac{\partial p}{\partial \mathbf{n}}|_{\text{inlet \& outlet}} = 0, \quad (2)$$

and boundary conditions on the airfoil are no-slip conditions:

$$\mathbf{v}|_{\text{airfoil}} = \mathbf{v}^{\text{ib}}, \quad \frac{\partial p}{\partial \mathbf{n}}|_{\text{airfoil}} = 0. \quad (3)$$

Here \mathbf{v}^{ib} is the velocity of the immersed boundary. The airfoil is rigid and it can oscillate with 1, 2 or 3 degrees of freedom. Its motion is described by dynamics equations:

$$\ddot{\vec{q}} = \vec{\Phi}(\vec{q}, \dot{\vec{q}}) + \vec{Q}^{\text{flow}} + \vec{Q}^{\text{ext}}. \quad (4)$$

Here \vec{q} is the airfoil generalized coordinates vector, $\vec{\Phi}(\vec{q}, \dot{\vec{q}})$ is determined by elastic and viscous constraints imposed on the airfoil, \vec{Q}^{flow} is the generalized aerodynamic force, \vec{Q}^{ext} is external mass generalized forces vector.

3 NUMERICAL METHOD

The Cartesian mesh with cells $\Omega_{i,j} = (x_{i-1}, x_i) \times (y_{j-1}, y_j)$ is introduced in the rectangular computational domain. It is denoted that $\Gamma_{i,j}$ is the face of $\Omega_{i,j}$ and $\vec{x}_{i,j}^c = (x_i^c, y_j^c)$ is the center of this cell. Unknown components $u_{i,j}$ and $v_{i,j}$ of velocity vector \mathbf{v} are computed in the middle of fluid parts of the cell faces. These points are the centers of control volumes $\Omega_{i,j}^u = (x_i^c, x_{i+1}^c) \times (y_{j-1}, y_j)$ and $\Omega_{i,j}^v = (x_{i-1}, x_i) \times (y_j^c, y_{j+1}^c)$ with faces $\Gamma_{i,j}^u$ and $\Gamma_{i,j}^v$ respectively (fig. 1).

Cells which the immersed boundary intersects are the so-called ‘cut-cells’ (fig. 2). These cells contain the solid part together with the liquid one. The level-set function φ is used for immersed boundary Γ^{ib} description. The boundary Γ^{ib} is represented by a line segment on the cut-cell $\Omega_{i,j}$. Location of this segment endpoints is defined by a linear interpolation of the variable $\varphi_{i,j} = \varphi(x_i, y_j)$.

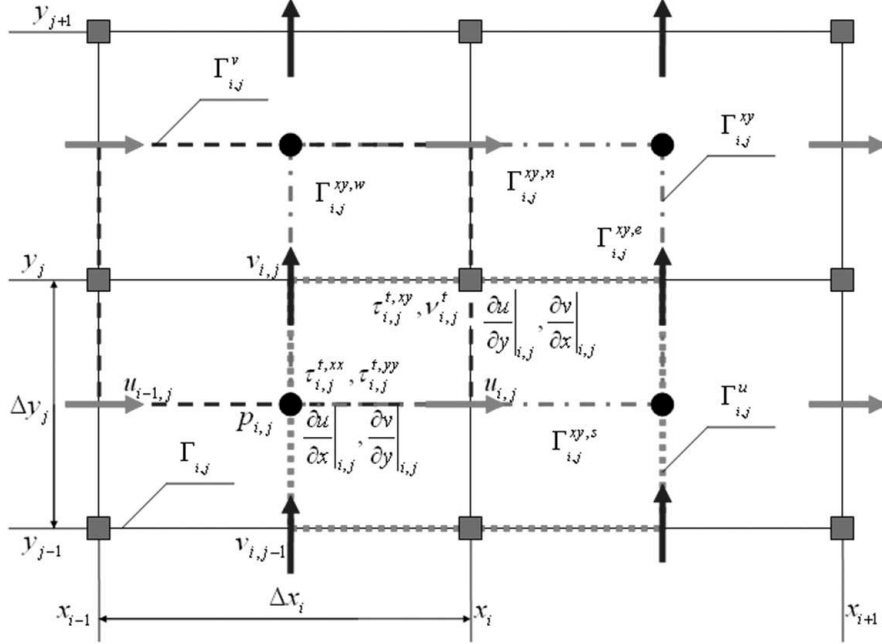


Figure 1: Staggered arrangement of the variables on the LS-STAG mesh

The cell-face fraction ratios $\vartheta_{i,j}^u$ and $\vartheta_{i,j}^v$ are introduced. They take values in interval $[0, 1]$ and represent the fluid parts of the east and north faces of $\Gamma_{i,j}$ respectively. One-dimensional linear interpolation of $\varphi(x_i, y)$ on the segment $[y_{j-1}, y_j]$ and $\varphi(x, y_j)$ on the segment $[x_{i-1}, x_i]$ is used for the cell-face fraction ratios computing:

$$\vartheta_{i,j}^u = \frac{\min(\varphi_{i,j-1}, \varphi_{i,j})}{\min(\varphi_{i,j-1}, \varphi_{i,j}) - \max(\varphi_{i,j-1}, \varphi_{i,j})}, \quad \vartheta_{i,j}^v = \frac{\min(\varphi_{i-1,j}, \varphi_{i,j})}{\min(\varphi_{i-1,j}, \varphi_{i,j}) - \max(\varphi_{i-1,j}, \varphi_{i,j})}. \quad (5)$$

According to the concept of the LS-STAG method normal Reynolds stress components are sampled on the base mesh (similar to pressure discretization) and shear ones are sampled in the upper right corners of the base mesh cells. Thus, for the shear Reynolds stresses an additional mesh (xy -mesh) is introduced. It is denoted that cell $\Omega_{i,j}^{xy} = (x_i^c, x_{i+1}^c) \times (y_j^c, y_{j+1}^c)$ is the control volume on the xy -mesh and $\Gamma_{i,j}^{xy}$ represents the faces of this control volume. In case of Reynolds Stress (RSM) RANS models, these meshes are used for transport equation solving for Reynolds stresses. The result then is taken into account in the Helmholtz equation for the velocity. In case of Eddy Viscosity (EVM) RANS models eddy viscosity is sampled on the xy -mesh. It is very suitable that the eddy viscosity at solid boundaries vanishes, so the cut-cells discretization of the eddy viscosity equations and computation of Reynolds stresses become simple.

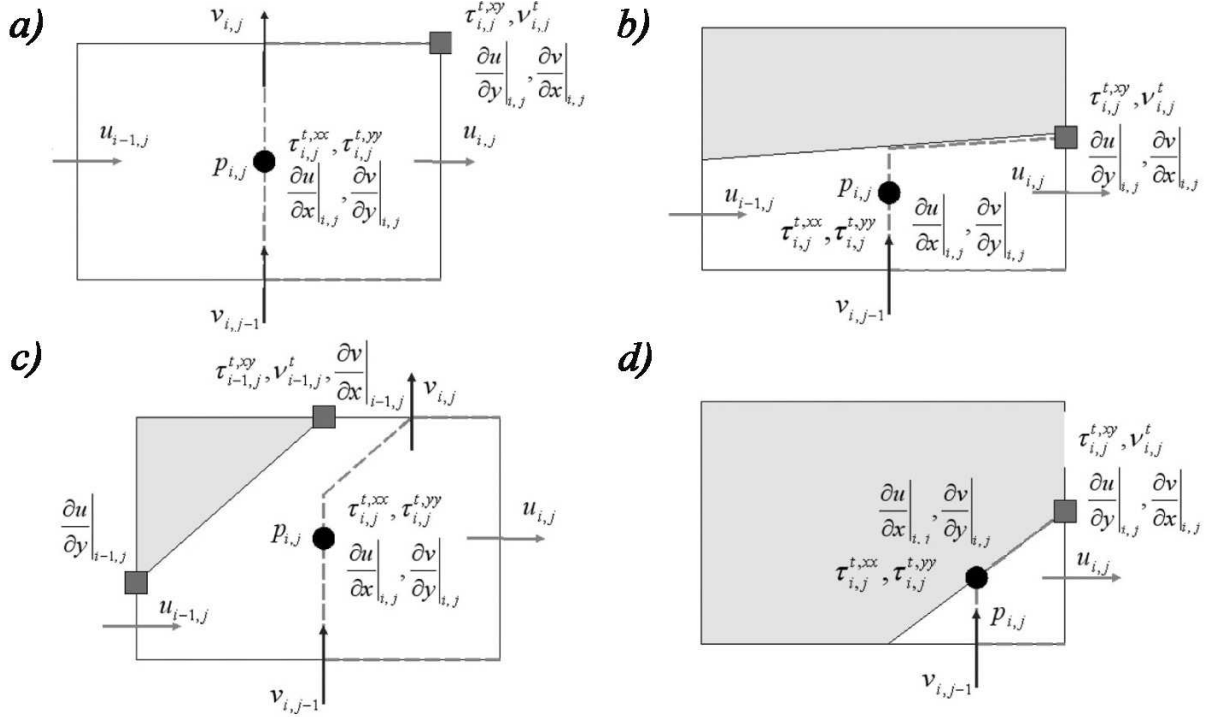


Figure 2: Location of the variables discretization points in the case of generic cells on the LS-STAG mesh: (a) Cartesian Fluid Cell; (b) North Trapezoidal Cell; (c) Northwest Pentagonal Cell; (d) Northwest Triangle Cell

4 NUMERICAL EXPERIMENTS

4.1 In-line oscillating circular airfoil in a free-stream

To validate the developed implementation of the LS-STAG method the flow past an in-line oscillating circular airfoil was computed. The in-line motion of the airfoil center is given by:

$$X_C = X_C^0 + \begin{cases} A, & t < 10D/V_\infty, \\ A \cos(2\pi S_e [tV_\infty - 10D]/D), & t \geq 10D/V_\infty, \end{cases} \quad (6)$$

$$Y_C = Y_C^0.$$

Here A is the amplitude of oscillations, S_e is the exciting Strouhal number, (X_C, Y_C) are coordinates of the airfoil center at the current time moment, (X_C^0, Y_C^0) are coordinates of the airfoil center at the initial time.

This problem has been numerically solved in [8, 9, 10] and it also has been studied by Dutsch et al. [11] in experiment with the following dimensionless parameters:

$$V_\infty = 1.0, \quad D = 1.0, \quad \text{Re} = 100, \quad A = 0.8D, \quad S_e = 0.2.$$

This flow is characterized by stable, symmetric and periodic vortex shedding.

Computations were performed on non-uniform grid 240×296 with time discretization step $\Delta t = 0.005$. Computed time averaged drag coefficient \bar{C}_x differs from the experimentally defined value [11] by less than 1% (table 1).

Table 1: Comparison of time averaged drag coefficient \bar{C}_x with established results from the literature

Mesh	\bar{C}_x	Mesh	\bar{C}_x
Dutsch (experiment) [11]		Guilmineau & Queutey [9]	
—	2.090	120×100	2.059
		120×200	2.063
The present study		180×100	2.069
240×296	2.075	180×200	2.072
		240×100	2.074
		240×200	2.078
		360×300	2.081
		480×400	2.080

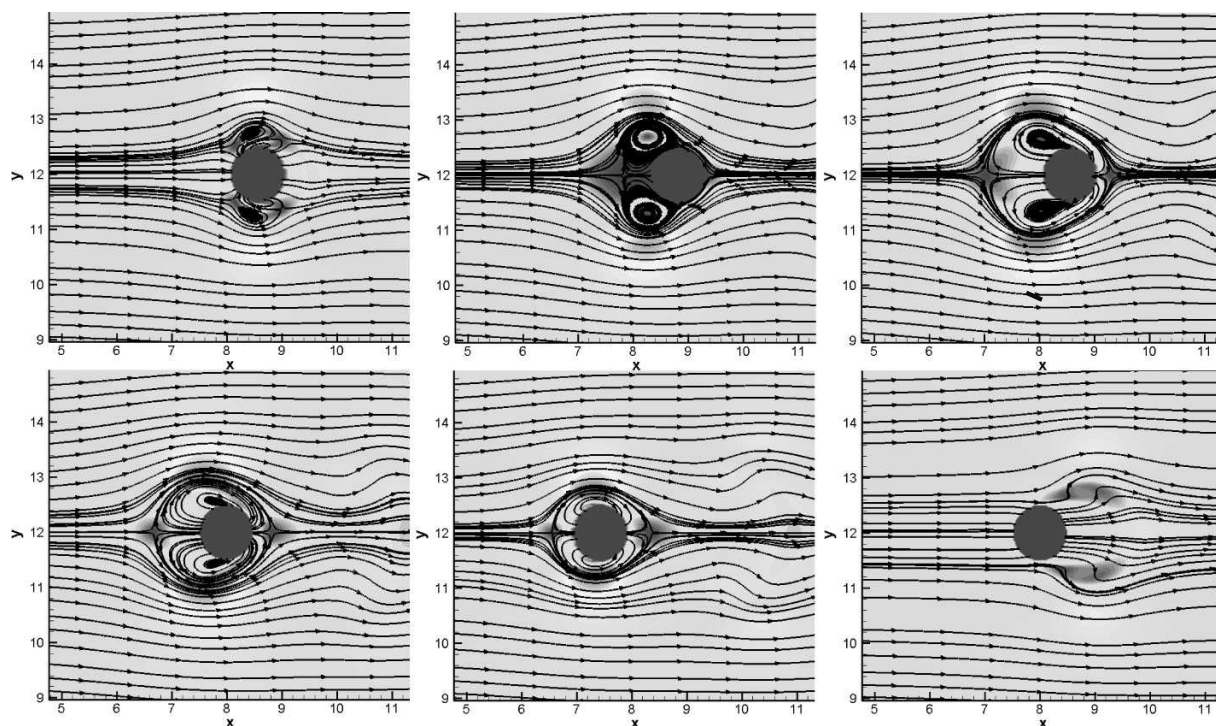


Figure 3: Dynamics of vortex formation and shedding from an in-line oscillating circular airfoil (the shown pictures correspond to sixth parts of the period)

Vortex dynamics is shown on fig. 3. As the airfoil moves from the initial position downstream, vortices begin to form on the top and bottom of it. Vortices increase in size when the airfoil is close to the rightmost position and reach their maximum radius when the airfoil is in the rightmost position. Then the airfoil starts its backward motion, creating the same vortex formation on the other side of it. As the direction of the airfoil motion changes again, the resulting pair of vortices is shedding from the airfoil. The described process begins again when the airfoil is returned to its initial position.

4.2 Circular airfoil wind resonance

To simulate wind resonance phenomenon we considered the motion of the circular airfoil with diameter D across the stream (with one degree of freedom). Airfoils constrain assumed to be linear viscoelastic and its motion (4) is described by the following ordinary differential equation:

$$m\ddot{y}_* + b\dot{y}_* + cy_* = F_y. \quad (7)$$

Here m is the airfoil mass, b is the damping factor, c is the constraint's elasticity, F_y is lift force, y_* is the deviation from the equilibrium. The natural frequency of the system $\omega \approx \sqrt{c/m}$ can be set by varying of the coefficient c .

The deviation from the equilibrium on the n -th step of computation is $y_*^n = Y_C^n - Y_C^0$. Here Y_C^0 is the ordinate of the airfoil center at the initial time and Y_C^n is the ordinate of the airfoil center at the n -th step of computation. Difference analogue of the equation (7) can be written down in the following form:

$$m \cdot \frac{Y_C^{n+1} - 2Y_C^n + Y_C^{n-1}}{(\Delta t)^2} + b \cdot \frac{Y_C^{n+1} - Y_C^{n-1}}{2\Delta t} + c \cdot (Y_C^n - Y_C^0) = F_y|_n. \quad (8)$$

Position of the airfoil center at the next time step can be easily obtained from this equation on each computation step after computing the lift force acting on the airfoil. It allows to reconstruct the level-set function and all matrices required for the computation and to compute the immersed boundary velocity \mathbf{v}^{ib} for recalculation the source terms.

Number of computations have been performed on non-uniform grid 272×292 with time discretization step $\Delta t = 0.0001$ and the following dimensionless parameters:

$$V_\infty = 3.0, \quad \rho = 1.0, \quad \nu = 0.003, \quad D = 1.0, \quad m = 39.75, \quad b = 0.731.$$

These parameters correspond to the Reynolds number $Re = 1000$. The dimensionless natural frequency of the system is the following:

$$Sh_\omega = \frac{\omega}{2\pi} \cdot \frac{D}{V_\infty} = 0.150 \dots 0.280.$$

Computational results are in good agreement with the previous studies [12]. Maximum amplitude (fig. 4) is about $0.4D$ and it occurs when the natural frequency of the system St_ω is close to the Strouhal number, calculated for a fixed airfoil $Sh \approx 0.24$ [2, 13, 14, 15].

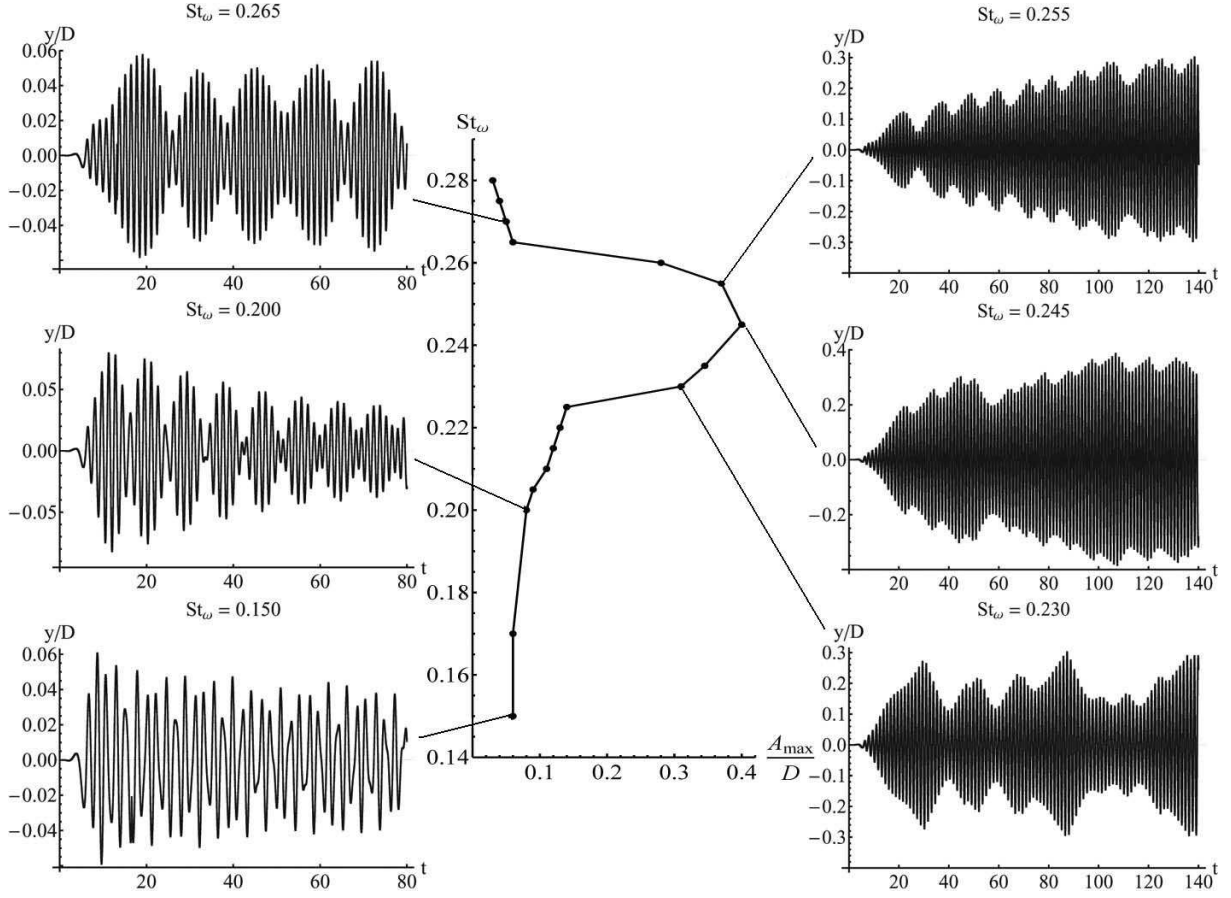


Figure 4: Maximum amplitude of the circular airfoil oscillations at $Re = 1000$

Qualitative differences in airfoil's dynamics at Strouhal numbers in investigated region are shown on fig. 4. Slight airfoil's vibration is observed when the natural frequency of the system is significantly less than the frequency of vortex shedding. Damped beats appear with increasing natural frequency as you get closer to the Strouhal number. Amplitude of the oscillations increases sharply near the frequency of vortex shedding. Beats disappear and amplitude continues to increase with time. Amplitude of the oscillations decreases sharply and beats are observed again with a further increase of the Sh_ω .

4.3 Wind turbine rotors autorotation

To simulate the rotation of wind turbine rotors, the following dynamics equation (4) has been solved:

$$I\ddot{\alpha} + k\dot{\alpha} = M^{\text{flow}}. \quad (9)$$

Here α is the rotation angle of the rotor, I is the polar moment of inertia of the rotor, k is the viscous friction coefficient in the axis, M^{flow} is the aerodynamic moment. Two-

dimensional problem is considered, so $M^{\text{flow}} = M_z$.

The rotor angular velocity is $\omega = \dot{\alpha}$. So difference analogue of the equation (9) can be written down in the following form:

$$I \frac{\omega^{n+1} - \omega^n}{\Delta t} + k\omega^n = M_z^n. \quad (10)$$

The aerodynamic moment on the n -th time step can be computed in the following way:

$$M_z^n = \sum_{\text{Cut-cells } \Omega_{i,j}^{ib}} [(x_i^C - X_C) F_{ya}^h|_{i,j}^n - (y_j^C - Y_C) F_{xa}^h|_{i,j}^n]. \quad (11)$$

Here (x_i^C, y_j^C) are coordinates of the center of $\Omega_{i,j}$ cell, (X_C, Y_C) are coordinates of the rotor center, around which the rotation takes place, $F_{xa}^h|_{i,j}^n$ and $F_{ya}^h|_{i,j}^n$ are the portion of drag and lift acting on the solid part of the cut-cell $\Omega_{i,j}$ on the n -th time step:

$$F_{xa}^h|_{i,j} = [n_x \Delta S]_{i,j}^{ib} \left(p_{i,j} - \nu \frac{\partial u}{\partial x} \Big|_{i,j} \right) - \nu \text{Quad}_{i,j}^{ib} \left(\frac{\partial u}{\partial y} \vec{e}_y \cdot \vec{n} \right), \quad (12)$$

$$F_{ya}^h|_{i,j} = -\nu \text{Quad}_{i,j}^{ib} \left(\frac{\partial v}{\partial x} \vec{e}_x \cdot \vec{n} \right) + [n_y \Delta S]_{i,j}^{ib} \left(p_{i,j} - \nu \frac{\partial v}{\partial y} \Big|_{i,j} \right). \quad (13)$$

Here $[n_x \Delta S]_{i,j}^{ib} = (\vartheta_{i-1,j}^u - \vartheta_{i,j}^u) \Delta y_j$, $[n_y \Delta S]_{i,j}^{ib} = (\vartheta_{i,j-1}^v - \vartheta_{i,j}^v) \Delta x_i$, $\Delta y_j = y_j - y_{j-1}$, $\Delta x_i = x_i - x_{i-1}$, $\text{Quad}_{i,j}^{ib}$ are the quadratures of the shear stress which depend on the cut-cells [2].

Value of the rotor angular velocity at the next time step can be easily computed after (10). New rotor position and the immersed boundary velocity can be defined by using this value:

$$\alpha^{n+1} = \alpha^n + \omega^n \Delta t, \quad (14)$$

$$\mathbf{v}_{i,j}^{ib,n+1} = \left\{ -\frac{y_j^C - Y_C}{|y_j^C - Y_C|} \cdot \omega^{n+1} |x_i^C - X_C|, \frac{x_i^C - X_C}{|x_i^C - X_C|} \cdot \omega^{n+1} |y_j^C - Y_C| \right\}.$$

It allows to reconstruct the level-set function and all matrices and the source terms required for the next time step.

Darrieus rotor (fig. 5) is the most interesting from the point of view of level-set function constructing from the types of rotors that we considered in this research. Symmetric TSAGI airfoil (fig. 6) has been used for modeling Darrieus rotor blade. The level-set function can not be constructed analytically for such shape rotor, as it was done for the circular airfoil and for simple rotor shapes, for example, for Savonius rotor (fig. 7). For this reason, it is necessary to approximate the Darrieus rotor boundary by a curve,

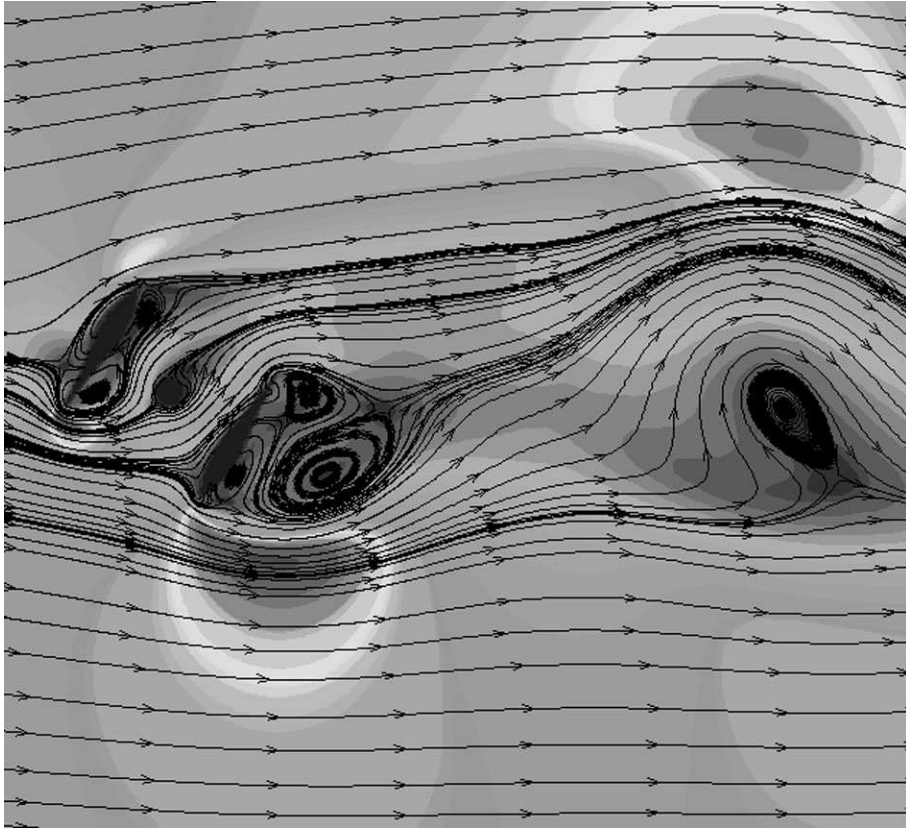


Figure 5: Darrieus rotor with two blades autorotation

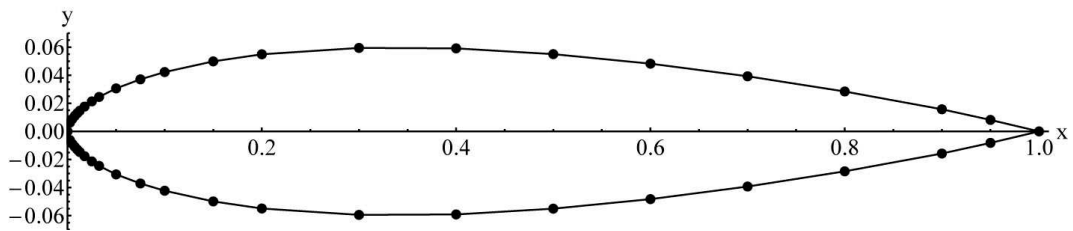


Figure 6: Symmetric TSAGI airfoil

which would make it possible to simulate both smooth parts of the boundary and the sharp edges. Furthermore, it is desirable that the distance from an arbitrary point to the boundary can be easily calculated. Construction of the level-set function for airfoil of arbitrary shape corresponding to these requirements is described in [15]. The basis of the developed algorithm is airfoil's boundary approximation by using Bezier curve.

To not reconstruct the Bezier curve for the airfoil boundary at each time step, the following approach can be used. At the beginning of the computation the Bezier curve and its derivative should be built for the rotor blade airfoil in position $\alpha = 0$. Then, the

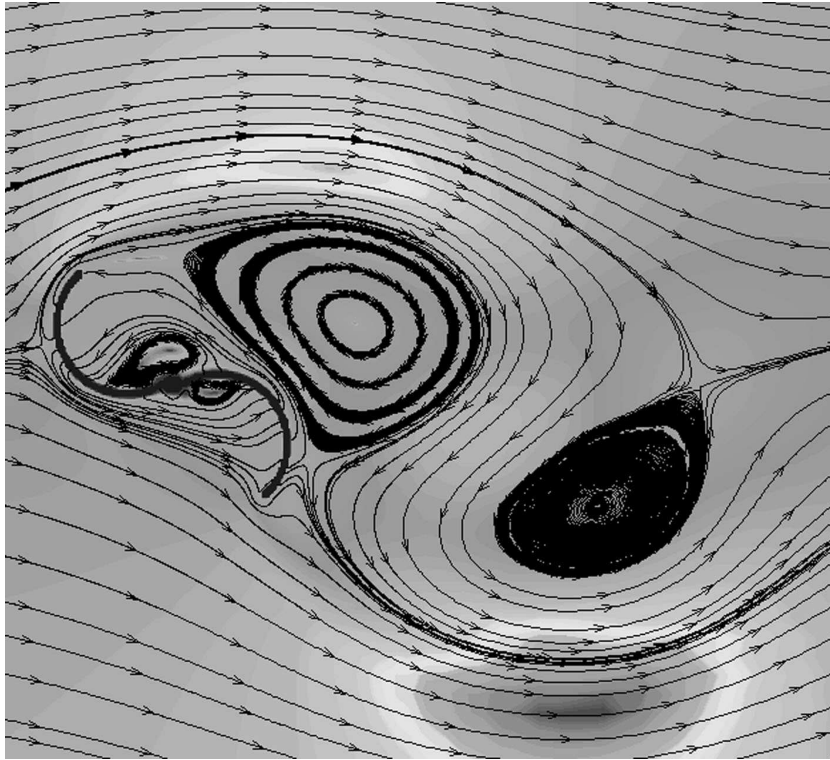


Figure 7: Savonius rotor with two blades autorotation

level-set function φ^n in point (x_i, y_j) can be computed as $\varphi^n(x_i, y_j) = \varphi^0(\tilde{x}_i, \tilde{y}_j)$ for the rotor rotated by angle α^n counterclockwise. Here φ^0 is the level-set function built for the rotor boundary in position $\alpha = 0$ by using the Bezier curve and $(\tilde{x}_i, \tilde{y}_j)$ is the point at which point (x_i, y_j) becomes upon rotation on α^n clockwise. Thus, the level-set function can be recalculated at any time without reconstructing the Bezier curve for each new rotor position.

5 CONCLUSIONS

- A software package is developed for the numerical simulation of the bodies' motion in the viscous incompressible flow by using the LS-STAG method.
- The general approach to the application of the LS-STAG method for the numerical solution of RANS equations is suggested by constructing the LS-STAG method extension with the Spalart — Allmaras turbulent model.
- Simulation of a circular airfoil wind resonance phenomenon and wind turbine rotors rotation and autorotation are considered.
- Computational results are in good qualitative agreement with the experimental data.

6 ACKNOWLEDGEMENTS

The work was partially supported by Russian Federation President Grant for young scientists [proj. MK-6618.2013.08].

REFERENCES

- [1] Mittal, R. and Iaccarino, G. Immersed boundary methods. *Annu. Rev. Fluid Mech.* (2005) **37**:239–261.
- [2] Cheny, Y. and Botella, O. The LS-STAG method: A new immersed boundary/level-set method for the computation of incompressible viscous flows in complex moving geometries with good conservation properties. *J. Comput. Phys.* (2010) **229**:1043–1076.
- [3] Osher, S. and Fedkiw, R.P. *Level set methods and dynamic implicit surfaces*. Springer, (2003).
- [4] Van der Vorst, H.A. Bi-CGSTAB: a fast and smoothly converging variant of Bi-CG for solution of non-symmetric linear systems. *SIAM J. Sci. Stat. Comp.* (1992). **2**:631–644.
- [5] Wesseling, P. *An introduction to multigrid methods*. John Willey & Sons Ltd., (1991).
- [6] Van Kan, J., Vuik, C. and Wesseling, P. Fast pressure calculation for 2D and 3D time dependent incompressible flow. *Numer. Lin. Alg. Appl.* (2000) **7**:429–447.
- [7] Marchevsky, I.K. and Puzikova, V.V. OpenFOAM iterative methods efficiency analysis for linear systems solving. *Proceedings of the Institute for System Programming of RAS.* (2013) **24**:71–86. [in Russian]
- [8] Udaykumar, H.S., Mittal, R., Rampunggoon, P. and Khanna, A. A sharp interface Cartesian grid method for simulating flows with complex moving boundaries. *J. Comput. Phys.* (2001) **174**:345–380.
- [9] Guilmineau, E. and Queutey, P. numerical simulation of vortex shedding from an oscillating circular. *J. Fluid Struct.* (2002) **16**:773–794.
- [10] Yang, J. and Balaras, E. An embedded-boundary formulation for large-eddy simulation of turbulent flows interacting with moving boundaries. *J. Comput. Phys.* (2006) **215**:12–40.
- [11] Dutsch, H., Durst, F., Becker, S. and Lienhart, H. Low-Reynolds-number flow around an oscillating circular cylinder at low Keulegan-Carpenter numbers. *J. Fluid Mech.* (1998) **360**:249–271.

- [12] Klamo, J.T., Leonard, A. and Roshko, A. On the maximum amplitude for a freely vibrating cylinder in cross flow. *J. of Fluids and Struct.* (2005) **21**:429–434.
- [13] He J.W., Glovinski, R., Metcalfe, R., Nordlander, A. and Triaux, J.P. Active control and drag optimization for flow past a circular cylinder. Part I: Oscillatory cylinder rotation. *J. Comput. Phys.* (2000) **163**:87–117.
- [14] Henderson, R.D. Nonlinear dynamics and pattern formation in turbulent wake transition. *J. Fluid Mech.* (1997) **352**:65–112.
- [15] Puzikova, V.V. Construction of Level-Set Function for an Airfoil of Arbitrary Topology when Modelling a Flow past It Using the LS-STAG Method. *Herald of the Bauman Moscow State Technical University. Natural Sciences.* (2012) **Special issue “Applied Mathematics”**:163–173. [in Russian]